CZECH TECHNICAL UNIVERSITY IN PRAGUE

Faculty of Nuclear Sciences and Physical Engineering

Department of Physics

Bachelor Thesis

Measurement of Silicon Particle Detector Properties

David Horák

Supervisor: Ing. Mária Čarná

Prague, 2013

ČESKÉ VYSOKÉ UČENÍ TECHNICKÉ
V PRAZE
Fakulta Jaderná a Fyzikálně Inženýrská
Katedra Fyziky

Bakalářská práce

Měření charakteristik křemíkových detektorů částic

David Horák

Vedoucí práce: Ing. Mária Čarná

Praha, 2013

Prohlášení:

Prohlašuji, že jsem svou bakalářskou práci vypracoval samostatně a použil jsem pouze podklady (literaturu, software, atd.) uvedené v přiloženém seznamu.

Nemám závažný důvod proti užití tohoto školního díla ve smyslu § 60 Zákona č.121/2000 Sb., o právu autorském, o právech souvisejících s právem autorským a o změně některých zákonů (autorský zákon).

V Praze dne ....

David Horák

Acknowledgement

I would like to express my gratitute to all who supported me during the creation of this work. I am very grateful to my supervisor Ing. Mária Čarná, for her willingness, patience, professional feedback and language corrections. I would also like to thank Ing. Michal Marčišovský for his valuable guidance, technical support and helpful consultations.

Abstract: This Bachelor's Degree project focuses on the measurement of radiation damage in CMOS test structures. The work summarizes the fundamental information about the silicon detectors, their properties and mechanisms of semiconductor radiation damage. Based on these information, results of measured data are presented and their analysis is given.

Key words: Silicon particle detectors, radiation hardness, CMOS technology, measurement of properties.

Abstrakt: Tato bakalářská práce se věnuje měření radiačního poškození v CMOS testovacích strukturách. Práce shrnuje základní informace o křemíkových detektorech, jejich vlastnostech a principech radiačního poškozování polovodičů. Na základě těchto informací jsou analyzována naměřená data a proveden jejich rozbor.

Klíčová slova: Křemíkové detektory částic, radiační odolnost, technologie CMOS, měření vlastností.

Contents

List of Figures

Chapter 1

Preface

Semiconductor particle detectors are widely used in a number of fields ranging from experimental particle physics to medicine and other practical applications. Development of semiconductor detectors is a logical outcome of radiation detection systems evolution, because they offer a multitude of advantageous properties such as compact dimensions, excellent energy and time resolution, low noise, cheap fabrication using industrial semiconductor processes and others. Semiconductor detectors became practically available in the early 1960s and they were called crystal counters. Currently, they are an essential part of the large detector systems such as ATLAS or CMS at the LHC.

In general, a semiconductor radiation detector consists of a semiconductor sensor and of a readout chip which processes small electrical signal from the sensor. This thesis discusses several topics related to semiconductor particle detectors. The practical part of this thesis concerns mostly the radiation damage of the electronic structures found inside of a readout chip. The first chapter presents a general overview of interactions of elementary particles in matter and methods of their detection. The properties of semiconductors, the use of a p-n junction as a particle detector and its properties are discussed in Chapter 2. The following chapter contains possibilities how to get information about the position of the interaction and the fabrication of position-sensitive detectors. In high energy particle physics, detectors are heavily damaged by radiation emerging in particle collisions, the mechanisms of this damage and improvement of detectors are discussed in Chapter 4. In the last chapter, results of the measurement of test structures characteristics both before and after irradiation are presented.

Chapter 2

Interaction of Particles with Matter

An understanding of the operation of a detector and radiation damage in a detector must be based on familiarity with fundamental mechanism of interaction of particles in matter. There are four major categories of particles characterized by their interaction - heavy charged particles, electrons, photons and neutrons.

2.1 Interaction of Heavy Charged Particles

Heavy charged particles, such as proton and alpha particle, interact with matter primarily via the electromagnetic interaction between their electrical charge and the charge of the orbital electrons. Interactions with nuclei are also possible, but occur rarely. In matter, heavy charged particle interacts with electrons, loses energy and possibly changes direction. The atomic electrons can be excited or removed from the atom (ionization).

The classical expression that describes energy loss in material is known as the Bethe formula[1] (Fig. 2.1) and is written as

$$\left\langle -\frac{dE}{dx} \right\rangle = 2\pi N_a r_e^2 mc^2 \rho \frac{Z}{A}\frac{z^2}{\beta^2}\left[\ln(\frac{2mc^2\gamma^2\beta^2 W_{max}}{I^2}) - 2\beta^2 - \delta - 2\frac{C}{Z}\right], \quad (2.1)$$

where r_e is the classical electron radius, N_a Avogadro´s number, ρ is the density of material, Z and A are the atomic number and the weight of material, I is the mean excitation energy, z is the charge number of the incident particle, W_{max} is the maximum energy transfer in a single collision, δ density correction and C is the shell correction.

[1] The Bethe formula is sometimes called Bethe-Bloch formula, Felix Bloch showed that $I = (10eV)Z$

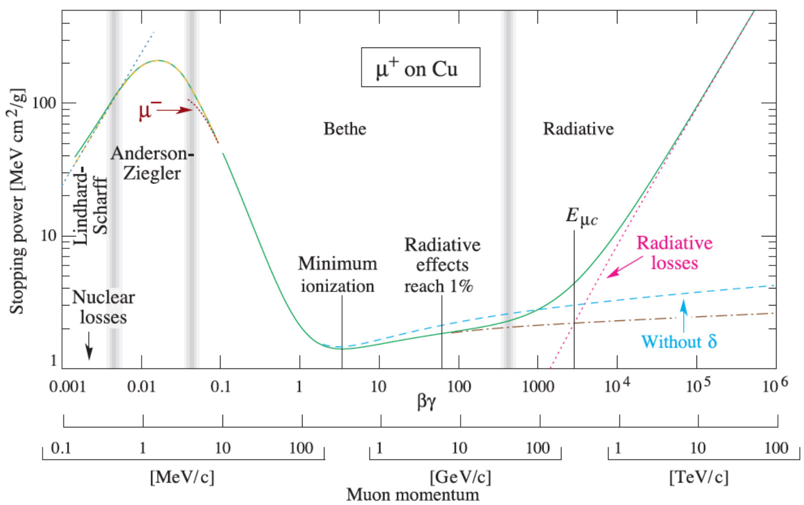

Figure 2.1: Average energy loss of a muon in copper. [4]

A plot of the specific energy loss along the track of charged particle is known as the Bragg curve. The peak with large energy deposits at the end of the track is called the Bragg peak.

2.2 Interaction of Electrons and Positrons

Electrons and positrons lose their energy by ionization, excitation and radiative processes (bremsstrahlung or electromagnetic radiation). The energy loss by ionization is described by the Bethe-Bloch formula similar to the one mentioned above.

The differential cross section for the electron-electron scattering at low energies is given by the Mott scattering formula, which can be found in [6]. At higher energies, the scattering is described relativistically by the so-called Møller's differential cross section. In this case the maximum energy transferred is $1/2$ of the incoming kinetic energy.

For collisions of positrons with high energy transfer the differential cross section is given by the Bhabha's formula, however, the maximum energy transfer is the whole incoming kinetic energy.

The acceleration and deceleration of the charged particle is accompanied by the emission of electromagnetic radiation. For circular accelerators it is called synchrotron radiation and in matter environment it is called bremsstrahlung. For electrons, with energies exceeding few tens of MeV, it is the dominant process of energy loss.

The probability of emission of radiation depends on the distance between the electron and the nucleus. When an electron passes far from the nuclei, the nuclear charge is screened by the atomic electrons.

The energy, at which both energy loss contributions are equal, is defined as the critical energy.

2.3 Interaction of Photons

There are three main mechanisms of photon interactions in matter - the photoelectric effect, the Compton scattering and the pair production. The differential cross section (Fig. 2.2) is given by the sum of these three contributions and strongly depends on the energy of interacting particle and on the traversed material.

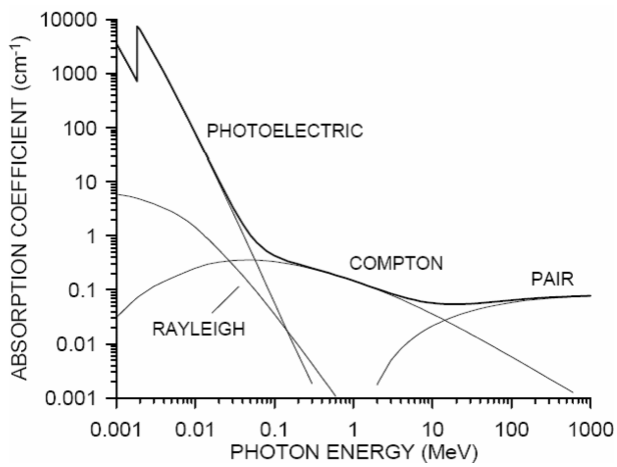

Figure 2.2: A photon total cross section for silicon.

2.3.1 Photoelectric Effect

At low energies, the main contribution to the total cross section is the photoelectric effect. When the energy of a photon is larger than the binding energy of an electron E_b, photon is absorbed in the interaction with atom and electron is emitted. The kinetic energy K_e of the emitted electron is given by:

$$K_e = h\nu - E_b, \tag{2.2}$$

where h is the Planck constant and ν is the frequency of the incident photon.

If the energy of photon is lower than the electron binding energy, electron cannot be emitted. It was an inexplicable phenomenon for classical physics. The electrons are located in shell orbits (K, L, M, ...) around the atom. When an electron is ejected from an atomic shell, a vacancy is created and the atom is left in an excited state. The atom can de-excite by emission of one or more electrons instead of a single photon. This process is called the Auger effect.

When the L-shell electron fills the K-shell vacancy, the difference between the K-shell and L-shell binding energies can be absorbed by an electron from higher shell and can cause its ejection. This electron is called the Auger electron.

2.3.2 Compton Scattering

In the Compton scattering process, an incoming photon of momentum $h\nu/c$ interacts with a free electron at rest. For photon with sufficient energy the electrons in the atom can be considered quasi-free. The incoming photon is reflected through an angle θ with respect to its original direction, and transfers some of its energy to the electron recoiled at the angle ϕ as shown in Figure 2.3.

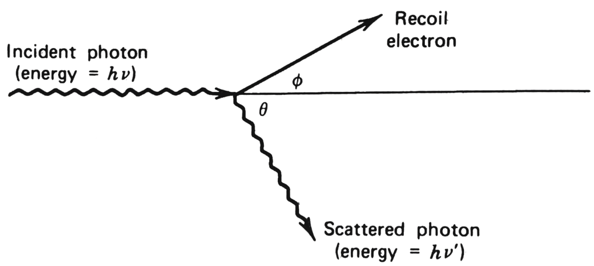

Figure 2.3: Compton scattering. [5]

Considering the momentum conservation, Compton has shown that the shift of electron's wavelength can be expressed as:

$$\Delta\lambda = \lambda' - \lambda = \lambda_e(1 - \cos\theta), \tag{2.3}$$

where $\lambda_e = \frac{h}{m_e c}$ is the Compton wavelength of the electron, θ is the scattering angle, λ is the initial wavelength, λ' is the wavelength after scattering and m_e is the rest mass of an electron. Equation 2.3 is called the Compton shift formula.

The differential cross section for the Compton scattering is described by the so-called Klein-Nishina formula [5]. The angular distribution of scattered photons is shown in Figure 2.4 and illustrates the strong tendency of forward scattering at high energies.

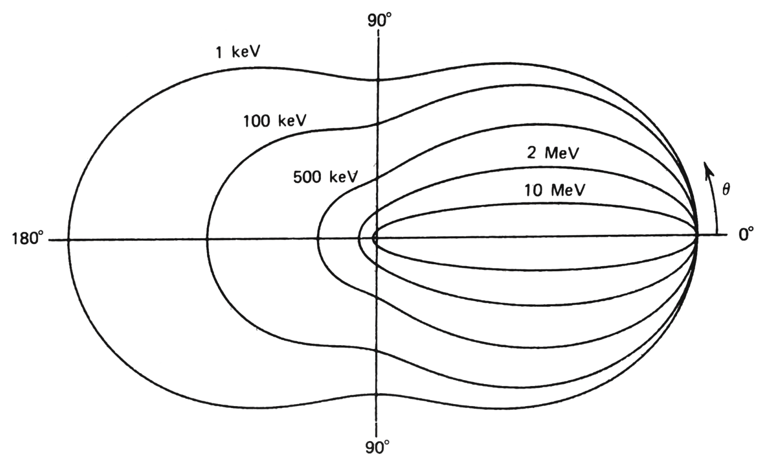

Figure 2.4: The angular distribution of scattered photons. [5]

2.3.3 Coherent Scattering

Another type of scattering, in which the photon interacts coherently with all the electrons of an absorber atom is called a coherent scattering. This scattering neither excites nor ionizes the atom, so the photon retains its original energy. [5]

2.3.4 Pair Production

The process of pair production is energetically possible, if the energy of the incoming photon exceeds twice the rest-mass of an electron (1,022 MeV). The process is possible only in the presence of the third charged particle (nucleus or atomic electron) which is necessary to preserve momentum.

In the interaction, the photon disappear and is replaced by an electron-positron pair. The excess energy of the photon is divided between the third particle and the produced pair. After slowing down in the surrounding material, the positron will annihilate, and two annihilation photons are created (secondary products of the interaction).

2.3.5 Electromagnetic Cascades

The phenomenon of electromagnetic cascades was first observed in high energy cosmic rays. A sketch of electromagnetic cascade can be seen in Figure 2.5.

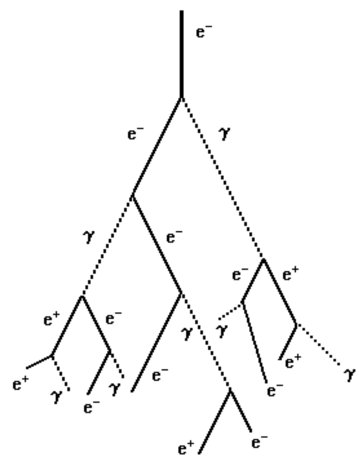

Figure 2.5: A sketch of an electromagnetic cascade. [2]

The incident high energy electron lost its energy by radiation via bremsstrahlung and therefore produced a high energy photon. This high energy photon loses its energy in the Coulomb field of nucleus via pair production or it produces a Compton electron. These electrons and positrons radiate new photons which again undergo pair production or Compton scattering. When a critical energy is reached, the particles lose their energy by collisions rather than by radiation and the cascade will stop.

2.4 Interaction of Neutrons

Neutrons are electrically neutral particles, and therefore cannot interact in matter via the electromagnetic interaction, which is the dominant energy loss process for charged particles. Neutrons interact only with the nucleus of the absorbing material.

There are various types of neutron interaction, which change with energy. Depending on the energy, interaction of neutrons can take the form of elastic or inelastic scattering, emission of the particle, neutron capture or fission of the nucleus.

The most common neutron converters (absorbers), used also in nuclear reactors or in nuclear medicine, are boron (or its compounds) and lithium.

2.4.1 Slow Neutron Detection

At low energies, neutron capture is the dominant process [5]. Neutron is absorbed by the nucleus and a gamma ray or a heavy charged particle (such as proton or alpha particle) are emitted. Most neutron detectors are based on some type of conversion process - the incident neutron is converted into a secondary charged particle, which can be detected directly.

The ^{10}B(n, α) Reaction

The ^{10}B(n, α) reaction is probably the most widely used reaction for conversion of slow neutrons into the directly detectable particles. The released energy Q is given by the equation:

$$^{10}_{5}\mathrm{B} + ^{1}_{0}\mathrm{n} \rightarrow \begin{cases} ^{7}_{3}\mathrm{Li} + ^{4}_{2}\alpha & Q = 2.792\,\mathrm{MeV}, \\ ^{7}_{3}\mathrm{Li}^{*} + ^{4}_{2}\alpha & Q = 2.310\,\mathrm{MeV}, \end{cases} \tag{2.4}$$

where the branching indicates that the ^{7}Li may be left in the ground state or in the first excited state. About 94% of all reactions lead to the excited state and the excited lithium returns to its ground state with a half-life of $\sim 10^{-13}$ s and with the emission of a 0.48 MeV photon. [11]

The ^{6}Li(n, α) Reaction

Another reaction useful for detection of slow neutrons is the ^{6}Li(n, α) reaction. This reaction may be written as:

$$^{6}_{3}\mathrm{Li} + ^{1}_{0}\mathrm{n} \rightarrow ^{3}_{1}\mathrm{H} + ^{4}_{2}\alpha \quad Q = 4.78\,\mathrm{MeV} \tag{2.5}$$

Figure 2.6 shows that the cross section is lower than for the ^{10}B reaction except in the resonance region. The lower cross section is a disadvantage, but it is offset by the higher Q-value. The lithium is also widely available in a separated form. [5]

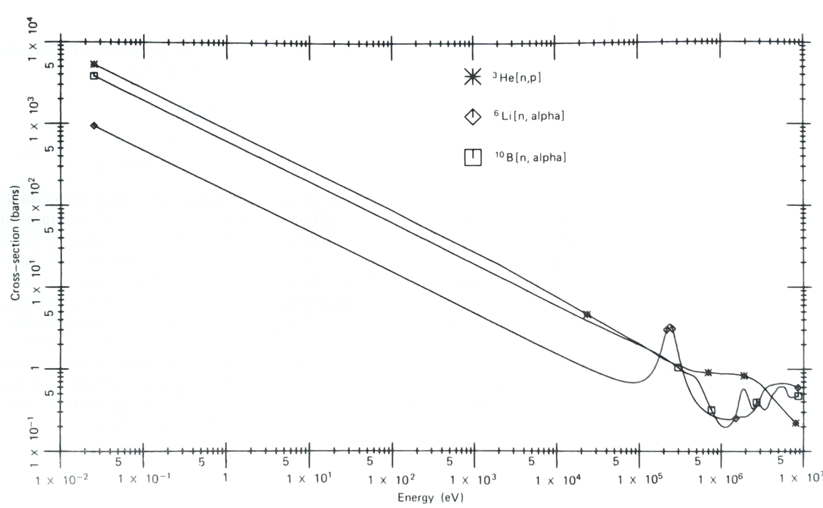

Figure 2.6: Cross section versus neutron energy for some reactions. [5]

The $^3\mathrm{He(n,p)}$ Reaction

^{3}He is also widely used for detection of slow neutrons. The reaction is written as:

$$^3_2\mathrm{He} + ^1_0\mathrm{n} \rightarrow ^3_1\mathrm{H} + ^1_1\mathrm{p} \quad Q = 0.764\,\mathrm{MeV} \tag{2.6}$$

The cross section (see Figure 2.6) for this reaction is significantly higher than that for the boron or lithium reaction; however, ^{3}He is relatively expensive for some applications and currently unavailable.

2.4.2 Fast Neutron Detection

At high energies, elastic scattering is the dominant process of energy loss. Neutron collides with a nucleus, changes direction and loses energy. The recoil nucleus is not excited (contrary to the inelastic scattering, where part of the energy is lost in exciting the nucleus). The cross section for the neutron elastic scattering on hydrogen is large and the entire energy of neutron can be transferred in a single collision, whereas only small fraction can be transferred in collision with heavy nuclei. Therefore, hydrogen is the most efficient moderator for fast neutrons.

All reactions mentioned in slow neutron detection are possible for fast neutrons as well, but the cross section for fast neutrons is very low as can be seen in Figure 2.6. Thus the detection efficiency is extremely small.

Most of the fast neutron detectors are based on neutron moderation using materials such as paraffin or PE foils.

Chapter 3

Introduction to the Silicon Particle Detectors

The use of semiconductor materials in particle detectors has many advantages. Semiconductor densities are 1000-times greater than gas densities, thus dimensions of semiconductor detectors can be smaller than dimensions of gas detectors. In addition, the semiconductor detectors have a lot of other advantages, such as fast timing or cheap fabrication, which will be mentioned below.

3.1 Semiconductor Properties

Semiconductor is a material which has higher electrical conductivity than an insulator and lower than a metal. The most important semiconductor materials used in detectors are silicon, germanium and cadmium telluride.

3.1.1 Band Structure in Solids

The band structure in solids describes ranges of energy that an electron may have and ranges of energy that are forbidden. A simplified representation of these energy bands can be seen in Figure 3.1.

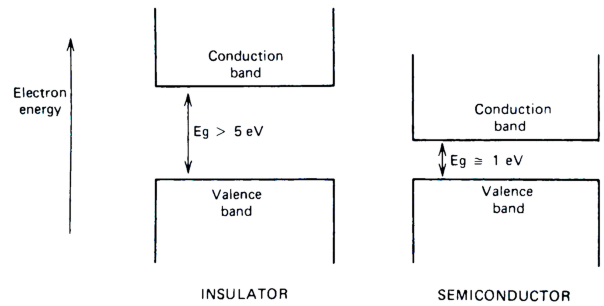

Figure 3.1: Band structure for electron energies in insulators and semiconductors. [5]

The lower band is called a valence band. It corresponds to the valence electrons, that are part of the covalent bonding within the crystal. The higher-lying band is called a conduction band and represents electrons that are free to move in the crystal lattice and that are responsible for the electrical conductivity of the material. Between these two bands is a bandgap. Its size determines the electrical properties of the material. For insulators, the bandgap is usually 5 eV [5] or more, while the bandgap for semiconductors is substantially smaller.

3.1.2 Charge Carriers

At nonzero temperature, a thermal energy is shared by the electrons in the crystal. It is possible that a valence electron gains sufficient thermal energy and is excited into the conduction band. This electron also leaves a vacancy (hole) in the valence band. Both can migrate through the crystal and are responsible for the observed conductivity of the material.

The probability, that an electron-hole pair is generated, is given by:

$$p(T) = CT^{\frac{3}{2}} \exp(-\frac{E_g}{2kT}), \tag{3.1}$$

where C is a constant characteristic of the material, T is the absolute temperature, k is the Boltzmann constant and E_g is the bandgap energy. As can be seen from Equation 3.1, the probability is significantly dependent on the ratio of the bandgap energy to the absolute temperature.

If an electric field is applied to the semiconductor material, both electrons and holes will move parallel to the direction of the applied field with a drift velocity. At low electric field intensity, the drift velocity v is a linear function of the applied field ε:

$$v = \mu\varepsilon, \tag{3.2}$$

where μ is the mobility of electrons and holes.

At higher electric field values, the drift velocity increases more slowly, and eventually a saturation velocity is reached with further increase in electric field.

Many semiconductor detectors are operated with electric field at which saturation velocity is reached. Because saturation velocity is of the order of 10^7cm/s, the time required to collect the carriers over the typical dimensions of 0.1 cm will be under 10 ns [5]. Therefore, semiconductor detectors are the fastest-responding of all detectors.

3.1.3 Intrinsic Semiconductors

An intrinsic semiconductor is a pure semiconductor without any dopants. It is also called an undoped semiconductor or an i-type semiconductor. At a temperature above absolute zero, some electrons will be excited across the band gap into the conduction band. Because each electron leaves behind a hole in the regular lattice, the number of electrons in the conduction band must be exactly equal to the number of holes in the valence band.

When a voltage is applied to the semiconductor, the current will flow and it will consist of two separate components: the current due to the flow of holes and that due to the flow of electrons. These two types of charge carriers move in opposite directions, but the total observed current will be their sum because of the opposite charges of holes and electrons.

The theoretical value of resistivity for intrinsic silicon at room temperature is $\rho = 230\,\Omega$cm [11], but in practice it is impossible to achieve this value because of residual impurities.

3.1.4 N-type Semiconductors

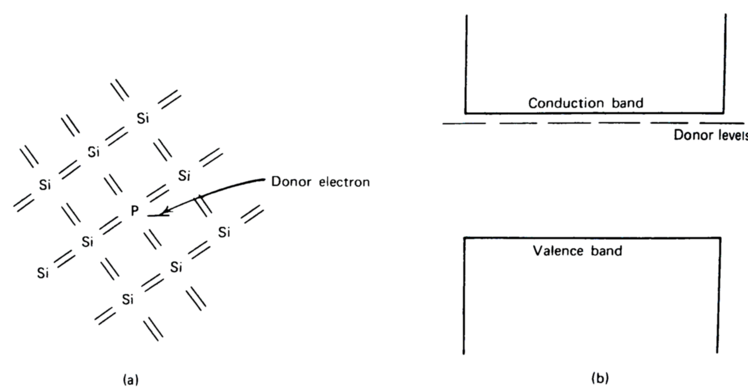

Figure 3.2: (a) Representation of a donor impurity (phosphorus). (b) Donor levels created in the silicon bandgap. [5]

When a small concentration of impurity is present, which is found in group V of the periodic table (so called donor impurities), the impurity atom will replace a normal silicon atom. Because there are five valence electrons surrounding the impurity atom and the silicon is tetravalent, there is one electron that is only lightly bound to the original impurity site. Therefore, the energy between these donor levels and the conduction band is small (see Figure 3.2), so that the probability of excitation is high and large fraction of these electrons skip into the conduction band.

The concentration of impurities is large compared with the concentration of electrons expected for the intrinsic material. Therefore, the number of conduction electrons is completely dominated by the concentration of the donor impurities. Higher concentration of electrons in the conduction band increases the rate of recombination, shifting the equilibrium between electrons and holes.

As a result, electrons are the majority charge carriers and holes are the minority charge carriers.

3.1.5 P-type Semiconductors

A small concentration of a trivalent (acceptor) impurity, which is found in group III of the periodic table (such as boron), results in a p-type conductivity. The impurity atom replaces a silicon atom in lattice. It has one less valence electron than silicon and therefore one covalent bond will be unsaturated. This vacancy represents a hole. If an electron is captured to fill this hole, it participates in the covalent bond, but it is slightly less attached as shown in Figure 3.3.

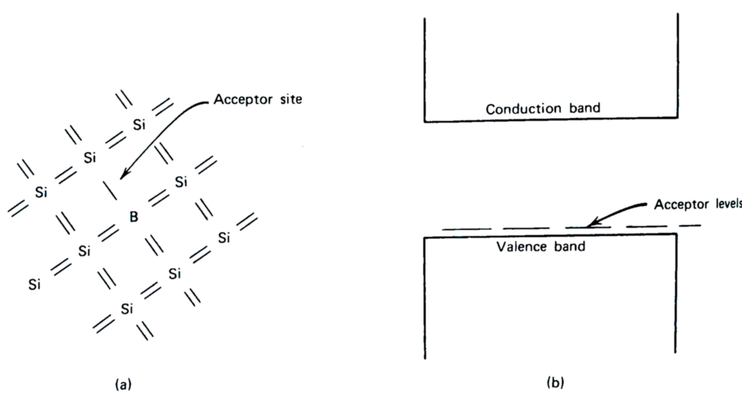

Figure 3.3: (a) Representation of an acceptor impurity (boron). (b) Acceptor levels created in the silicon bandgap. [5]

In the p-type material, holes are the majority carriers and electrons are the minority carriers.

3.1.6 Compensated Material

The material is compensated, when donor and acceptor impurities are present in equal concentration. This material has some of the properties of an intrinsic semiconductor. In practice, it is impossible to achieve an exact compensation at the time of fabrication, because any small imbalance in donor or acceptor concentration leads to n- or p-type behavior as shown in Figure 3.4. The only way to gain a compensated material is through the lithium ion drifting in a p-type monocrystal.

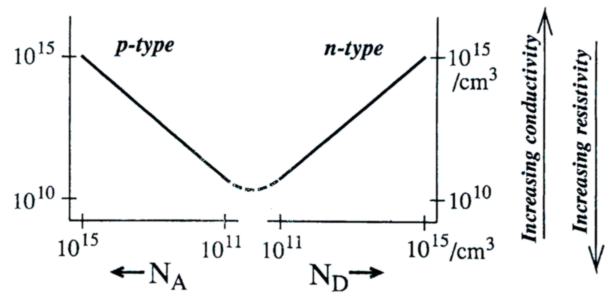

Figure 3.4: Conductivity of a semiconductor as a function of the concentration of acceptors (N_A) and donors (N_D). Logarithmic scales. [5]

3.1.7 Heavily Doped Material

Thin layers of semiconductors, that have very high concentration of impurities (n^+, p^+), have very low minority carrier density. Thus, these layers are often used in making an electrical "blocking" contact.

3.2 The p-n Junction as a Detector

An intrinsic semiconductor cannot be used as a detector because of high value of thermal current. The one possibility of reducing the thermal current in a semiconductor is to use a junction between n- and p-type semiconductor material (p-n junction). The p-n junction cannot be created by simply pressing together two pieces of material, because gaps will be large compared with the interatomic lattice spacing. Therefore, the junction is formed in a single crystal by changing the impurity concentration by diffusion or ion implantation.

The p-n junction is well-known in its role as a diode. The junction conducts current when a voltage is applied in the "forward" direction (positive voltage is applied to the p side), but it will conduct very little current when biased in the "reverse" direction. In the "forward" direction, the majority charge carriers migrate through the junction, which the current flows through and therefore cannot be used as a detector.

3.2.1 Reverse Bias Junction

Some properties of the reverse bias junction can be derived from a simple charge distribution sketched in Figure 3.5. On the left side of the junction is a p-type semiconductor, on the right side is a n-type semiconductor. The majority charge carriers were removed by the electric field (the depleted region is created) and the minority charge carriers can be ignored.

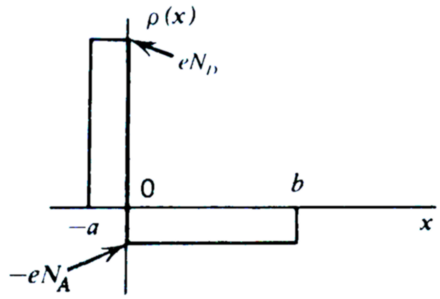

Figure 3.5: Charge distribution. [5]

The electric field and electric potential can be calculated by solving the Poisson's equation:

$$\frac{\mathrm{d}^2\varphi}{\mathrm{d}x^2} = \begin{cases} -\frac{eN_D}{\varepsilon_r\varepsilon_0} & (-a < x \leq 0) \\ +\frac{eN_A}{\varepsilon_r\varepsilon_0} & (0 < x \leq b) \end{cases} \tag{3.3}$$

The corresponding shape of the electric field is shown in Figure 3.6.

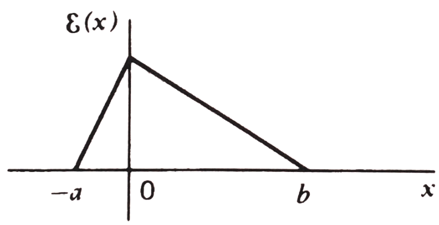

Figure 3.6: Electric field in p-n junction. [5]

The sketch of the electric potential is in Figure 3.7.

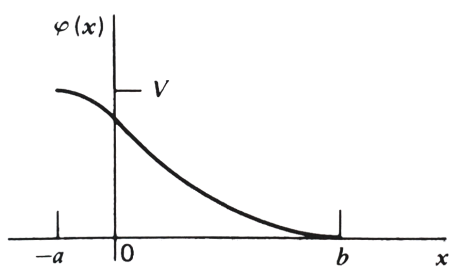

Figure 3.7: The sketch of the electric potential in p-n junction. [5]

The total width of the depletion region d can be expressed as:

$$d \cong (2\varepsilon_r \varepsilon_0 V \mu \rho_D)^{1/2}, \tag{3.4}$$

where V is the applied bias voltage, μ is the mobility of the majority charge carrier and ρ_D is the resistivity of the doped semiconductor. As can be seen, the largest depletion width for a given voltage can be achieved by using the material with the highest resistivity. This resistivity is limited by the purity of the undoped material. Therefore, it is important to make detectors from the highest purity material available.

The depleted region has properties of a capacitor with the value of the capacitance:

$$C \cong S \left(\frac{e\varepsilon_r \varepsilon_0 N}{2V} \right)^{1/2}, \tag{3.5}$$

where S is the surface of the detector and N represents the dopant concentration on the side of the junction that has the lower dopant level. A small value of the detector capacitance reduces the electronic noise, and thus it is important for good energy and timing resolution. As can be seen, it is promoted by using the largest applied voltage possible.

3.3 Operational Characteristics

3.3.1 Maximum Operating Voltage, Breakdown Voltage

The maximum operating voltage is limited by the breakdown voltage, which causes a large increase in current that deteriorates the properties of a detector and usually damages the detector permanently. The breakdown voltage is an individual characteristic of a detector and can not be predicted in advance. The maximum operating voltage is usually in the range of 100-1000 volts [11].

3.3.2 Leakage Current

When a reverse bias voltage is applied to a junction detector, a small current of the order of a nanoampere (dependent on the geometry and technology used) is observed. This leakage current is related both to the bulk volume and to the surface of the detector.

There are two mechanisms, which cause the increase in the bulk leakage current. In a reverse bias, the majority charge carriers will be repelled away from the junction. However, the minority carriers are attracted and will be conducted across the junction.

A second source of the bulk leakage is the thermal generation of the electron-hole pairs in the material as was discussed in section 3.1.2. The generation rate is proportional to the volume of the depleted region and can be reduced by cooling the detector. Because silicon detectors have sufficiently low thermal generation, they can be operated at room temperature, but germanium detectors must always be operated at reduced temperatures [11].

Surface leakage effects take place at the edges of the junction. However, in detectors produced by the planar fabrication process, the surface leakage current is reduced to a small fraction of that observed in the diffused junction and surface barrier devices. [5]

Monitoring the leakage current can detect any abnormal detector behavior. During operation, the leakage current should maintain a steady value and any change in the leakage current can indicate a detector degradation. Sudden increase can signal the approach of the breakdown of the diode. Eventually, the long-term behavior of the leakage current can be used to monitor the degree of radiation damage as will be discussed below.

Chapter 4

Position-Sensitive Semiconductor Detectors

In this chapter, the basic types of the position-sensitive semiconductor detectors and their fabrication will be discussed.

4.1 Types of Position-Sensitive Semiconductor Devices

Position-sensitive detectors have applications in many different areas, for example medicine or high energy particle physics. There are several design approaches possible, which are able to obtain the information about the position of the impacting particle.

4.1.1 Microstrip Detectors

A microstrip detector is the basic position-sensitive detector. One of the electrodes is divided into thin parallel strips as illustrated Figure 4.1.

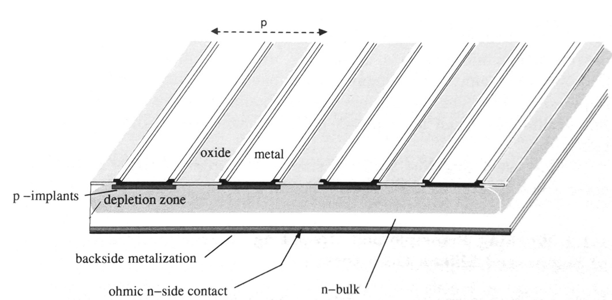

Figure 4.1: Sketch of a single-sided microstrip detector. [12]

These strips are fabricated on one surface using the ion implantation and photolithographic techniques, which will be discussed below. Detectors have been produced with strips widths as small as 10 μm [11]. One of the charge carrier created within the depleted region of the detector will travel to the closest strip and the strongest signal will be observed on this strip. Thus each strip must be connected independently to the charge processing electronics.

To obtain two-dimensional information, a double-sided strip detector can be produced. The strip electrodes are placed in orthogonal orientation on the opposite sides of the wafer. The x and y coordinates are obtained by the independent electrons and holes travelling in opposite direction.

4.1.2 Pad or Pixel Detectors

To obtain two-dimensional position information, a grid of small detectors that are electrically isolated from each other can be fabricated. When the dimensions of an electrode are one millimeter or larger, it is called a pad detector, whereas for electrode dimensions smaller than one millimeter, it is called a pixel detector [5]. The small size of electrodes results in a small capacitance and leakage current, and thus the noise is reduced in comparison with the microstrip detectors.

Connecting each pixel to the readout electronics is a challenging technical task. Usually, a pixel chip is connected to a separate readout chip using the flip chip solder bonding or indium bump bonds [5].

An active area of semiconductor detector is usually of the order of cm^2. Larger detector area can be achieved by attaching the detectors next to each other. However, this process is expensive, complex to evaluate and develop electronics for such complex devices, so microstrip detectors usually provide to be a better alternative.

4.1.3 Semiconductor Drift Detectors

In a semiconductor drift detector, the drift time of the charge carriers is used to deduce the position of the interaction. A special electrode configuration of this type of detector is illustrated in Figure 4.2. Electrons formed by the interaction are transported parallel to the surface and collected on the anode near the edge of the wafer. Another geometry such as cylindrical is also possible. The advantage of a drift detector is a small area of the anode, which is crucial for its capacitance and thus the noise level, energy and time resolution of the drift detector is excellent.

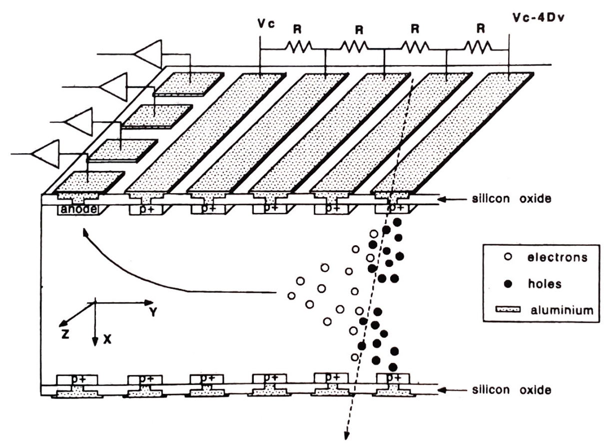

Figure 4.2: Structure of a silicon drift detector. [5]

4.1.4 Charge Coupled Devices

Charge coupled devices (CCDs) were primarily designed for detection of visible light. However, they can be extremely useful as sensors for radiation detection and imaging. A schematic diagram of a simple linear CCD can be seen in Figure 4.3.

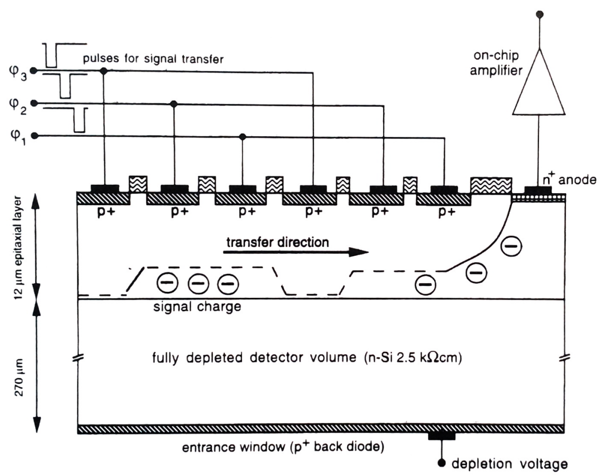

Figure 4.3: A schematic diagram of a linear CCD chip. [5]

A depletion region is created below the front surface, and a potential minimum for electrons is created a few microns below the surface, which consists of a metal-oxide-silicon (MOS) electrode structure or a p-n diode structure. The trapped electrons are collected by an anode at the edge of the wafer.

A two dimensional detector is obtained by attaching a couple of linear CCDs in parallel, which are readout by another linear CCD as illustrated in Figure 4.4.

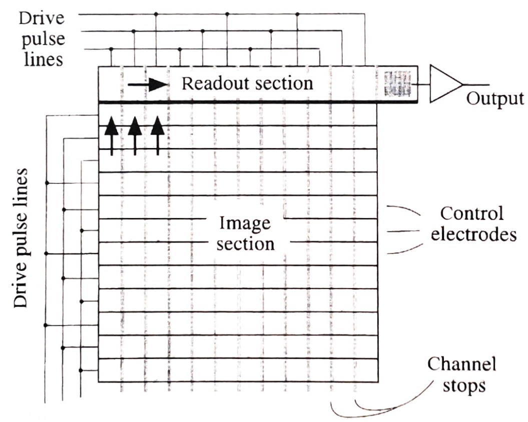

Figure 4.4: Layout of a two-dimensional CCD. [5]

4.2 Detector Fabrication

In this section, the key steps of detector fabrication will be discussed. This process is derived from the planar technology developed for microelectronics and thus profits from its research. An example of production can be seen in Figure 4.5 and will be described below.

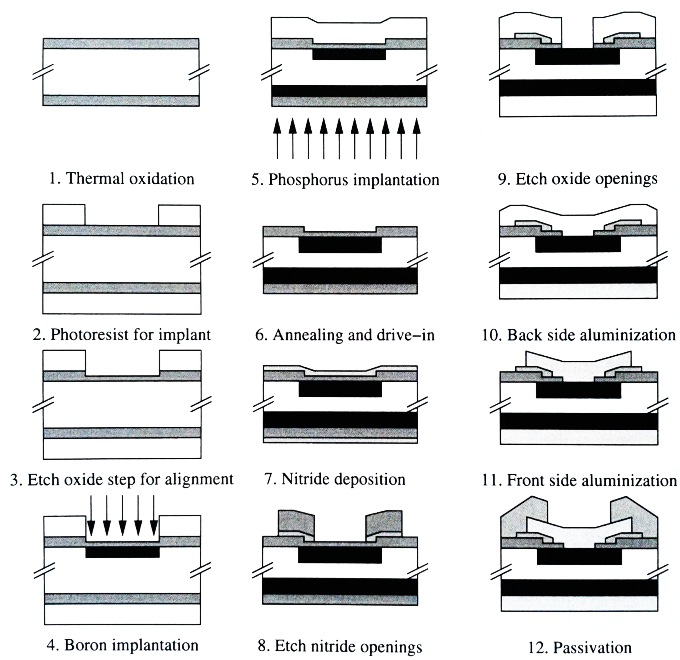

Figure 4.5: An example of production of a sensor. [12]

4.2.1 Wafer Production

The first step is the production of wafers. Silicon is isolated from quartzite by reduction with carbon at temperatures above 1400°C. This silicon is then converted to form trichlorosilane ($SiHCl_3$) and boiled. The boiling point of impurities is higher so the trichlorosilane is cleaned and transformed back to solid silicon. This material is used to grow large crystals. There are two common growing methods.

The Czochralski method can be seen in Figure 4.6. The silicon melt is contained in a crucible. A seed crystal is pulled under rotation from the surface of the liquid. The silicon freezes out at the surface. The diameter of the ingot can be modified by the speed of rotation.

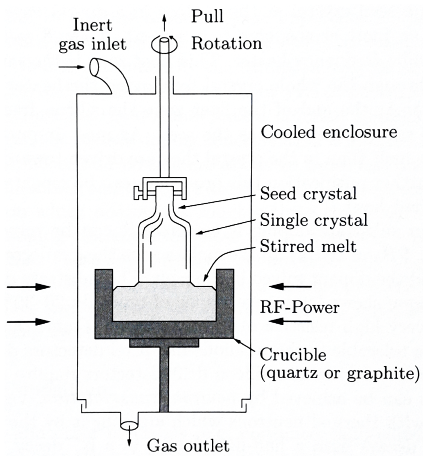

Figure 4.6: Schematic diagram of a Czochralski process. [12]

However, the Czochralski-grown silicon can not be used for applications requiring a resistivity higher than $10\,\Omega$cm because of many impurities [12].

Detectors, for which a high resistivity is needed, can be produced using the float zone (FZ) method. As shown in Figure 4.7, a high-purity silicon rod is vertically mounted in an inert gas atmosphere. A small zone of the rod is melted by the radio-frequency heater. This is called the float zone and it is moved from the seed crystal to the top by moving the RC heater slowly upward and the silicon freezes out as a single crystal. Since most impurities are better solvable in the melt than in the crystal, they are driven toward the end of the ingot [12]. This process can be repeated several times for further purification.

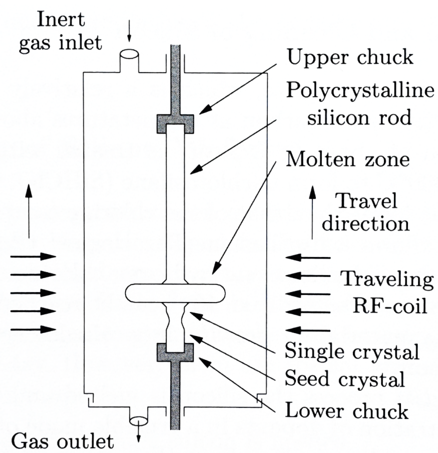

Figure 4.7: Schematic diagram of a float zone process. [12]

The crystal ingots are cut into wafers which are lapped and polished.

4.2.2 Thermal Oxidation

The next step is usually thermal oxidation of the wafer surface (Figure 4.5-1.). Silicon oxide is grown by storing the wafer at a high temperature (between 900 and 1200°C [13]) in an oxygen atmosphere. It is called dry oxidation. If faster growth is required, water vapor is added to the atmosphere, this process is called wet oxidation. However, slow growth usually provides quality in breakdown stability, surface changes and other properties. Thin gate oxides in the MOS electronics are usually grown at lower temperature (around 800°C [12]).

Thermal oxidation provides protection of the wafer surface and also provides good termination of the silicon crystal. [12]

4.2.3 Patterning

For patterning of a wafer, a technique called photolithography is used. A photosensitive material (photoresist) is dropped in the center of the wafer and is distributed by the fast rotation of the wafer. The photoresist is illuminated through a mask, usually a chrome pattern on a glass substrate. For a good resolution, a short wavelength in the UV range is used. Then the illuminated areas (positive resist, more common) or nonilluminated areas (negative resist) are removed, and therefore exposed to etching or implantation.

4.2.4 Etching

Copying the structure of the photoresist into the underlaying layers and removing the material is done by etching. There are two types of etching, wet etching and dry etching.

Wet etching is commonly used in sensor processing. The wafer is immersed in a bath. This leads to an underetching of the mask; however, it is not a problem due to the relatively small sizes.

In microelectronics, dry plasma etching is the most widely used method. It provides a high degree of anisotropy, and therefore allows creation of small structures unlike the wet etching. However, the plasma induces radiation damage in the oxides, so this process is inappropriate in the sensor technology.

4.2.5 Doping

There are two methods to introduce dopants into the silicon surface - diffusion and implantation. Boron is the most common p-dopant, whereas phosphorus and arsenic are typical n-dopants.

Diffusion

During diffusion doping, the wafer is exposed to dopants in the form of gas at the temperatures of 800-1200°C [12]. Higher temperatures accelerate the diffusion process, so the depth depends on the duration, concentration and temperature.

Ion Implantation

Ion implantation is currently the most commonly used doping method. The doping atoms are ionized, accelerated by an accelerator (10-15 kV [11]) and shot into the silicon wafer. The penetration depth of the ions and the shape of the doping profile can be adjusted by choosing the accelerating voltage.

After implantation, ions are in interstitial sites in the crystal lattice, so they are not electrically active. In addition, the crystal is damaged by the implantation, thus thermal annealing is required. However, the temperature (500°C [11]) is substantially lower than the temperature required for diffusion, so the material is not as damaged as by the diffusion process.

4.2.6 Metallization

The metallization (Figure 4.5-10.,11.) provides a low resistivity connection between devices on the same silicon substrate. The most common metal used for metallization is aluminium (aluminization process), because of its low resistance and its good adhesion on silicon oxide [12]. The metal can be sputtered or evaporated. A good ohmic contact is possible only if the silicon is highly doped on the contact. Also a sintering step is necessary.

4.2.7 Surface Passivation

The final step of detector production is usually surface passivation (Fig. 4.5-12.). The silicon surface must be protected against mechanical damage and chemical contamination. Thermally grown silicon dioxide is ideal for this purpose. It is used for the gate insulator in metal oxide semiconductor field effect transistors

(MOSFETs) and as the surface passivation between strip or pixel detectors, where it is a crucial step.

Oxides can be thermally grown by a process called chemical vapor deposition - the wafers are exposed to gaseous ambient in high temperature furnaces.

4.3 CMOS Technology

Complementary metal-oxide-semiconductor (CMOS) is a technology for fabrication of integrated circuits, microprocessors and logic circuits.

4.3.1 Metal Oxide Semiconductor Structure

The metal oxide semiconductor (MOS) structure is the basic unit of the MOS field effect transistor, which is widely used in microelectronics. The MOS structure is often used in strip sensors as a coupling capacitor and in charge coupled devices for charge storage. In pixel detectors, understanding MOS structures is important to deal with the consequences of radiation-induced surface damage, which will be discussed in the next chapter.

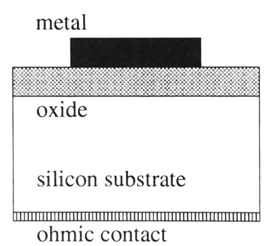

Figure 4.8: Schematic diagram of a MOS structure. [12]

A schematic diagram of a MOS structure can be seen in Figure 4.8. When a bias is applied between the silicon substrate and the metal (which is called the gate), no current will flow thanks to the insulating oxide layer [12]. However, if a positive voltage is applied, electrons in the MOS structure on a n-type silicon will be attracted to the gate and an accumulation layer will be created. If the voltage is negative, the electrons are pushed to the bulk and a depletion zone is formed. The situation on a p-type silicon is exactly the opposite. The MOS structure operates essentially as a capacitor.

4.3.2 MOS Field Effect Transistors

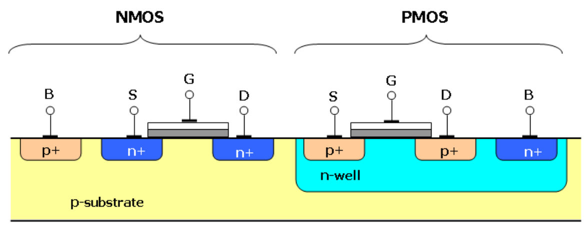

Figure 4.9: Schematic structure of a MOSFET. [15]

A sketch of a metal-oxide-semiconductor field effect transistor (MOSFET) can be seen in Figure 4.9. There are two types of MOSFET - NMOS and PMOS [10]. The former is created in a p-substrate, whereas the latter is placed in a n-well.

In NMOS, the two electrodes are formed by n^+ regions and are usually called source and drain. The gate is created between source and drain electrodes and is insulated by an oxide. A conducting channel is formed by applying a positive voltage to the gate electrode.

Chapter 5

Mechanisms of Radiation Damage

In this chapter, various mechanism of radiation damage of silicon detectors and their consequences will be discussed. Radiation damage in silicon detectors is usually divided into bulk and surface damage.

5.1 Bulk Damage

Bulk damage forms a significant part in the radiation damage of a sensor, whereas in electronics it does not play an important role due to the high dopant concentration and thin active volume.

5.1.1 Damage Mechanism

Bulk damage is primarily caused by displacement of a silicon atom from its lattice site. To remove the silicon atom a minimum energy of approximately 25 eV is required. The displaced atom is called a primary knock on atom (PKA). By this process interstitials and vacancies (Frenkel pairs) are created. They are not stable, they can propagate through the crystal lattice. If the energy transferred to the PKA is high enough, further silicon atoms can be displaced. For example, a 1 MeV neutron transfers the energy of about 60 - 70 keV, which leads to the displacement of approximately 1000 atoms [13]. As can be seen in Figure 5.1, the displacement of atoms acts as a cascade and at the end of the path of the knocked off atoms disordered regions (called clusters) emerge.

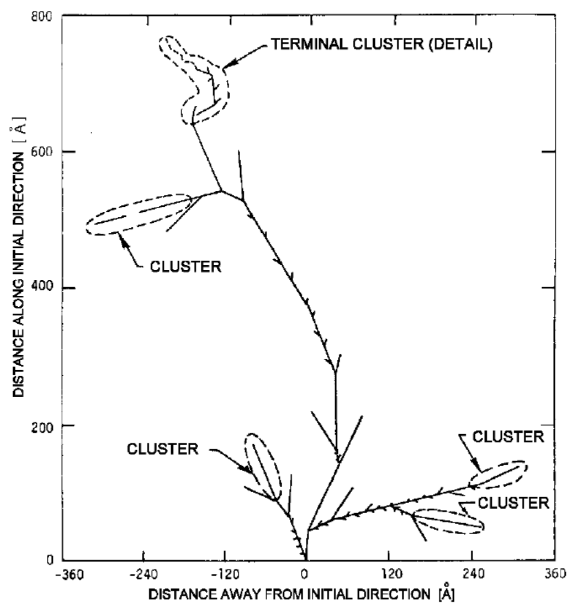

Figure 5.1: Monte Carlo simulation of a recoil-atom track with a primary energy of 50 keV. [9]

5.1.2 The NIEL Hypothesis

The displacement damage is caused primarily by hadrons and high energy photons. The radiation damage is scaled with the nonionizining energy loss (NIEL), which depends on the particle type and energy. The NIEL hypothesis is expressed by the so-called damage function, which is shown in Figure 5.2. The damage is related to 1 MeV neutron damage.

The minimum energy for neutron displacement by elastic scattering is 190 eV [9]. Below this value (lower energy), the cross section rises due to the neutron capture and emission of gamma rays. However, for high energy experiments it does not play a significant role. On the other hand, the proton cross section is much larger at lower energies, because the proton damage function is dominated by the Coulomb interaction. At high (GeV) energies, both damage functions approach a common value. The interaction of pions is influenced by the delta resonance around a few hundred MeV, but in the high energy limit the damage function tends to be about 2/3 (quark weighting factor) of proton [9]. X-rays do not cause direct displacement damage, but electrons from photoelectric effect, Compton scattering and pair production can cause point defects. Therefore, gamma rays with energy greater than 250 keV are a perfect source for investigation of point defects [3].

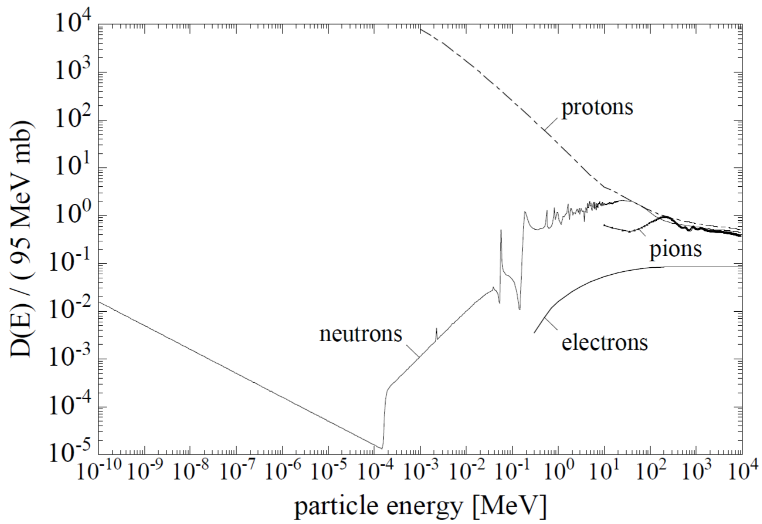

Figure 5.2: Displacement damage function D(E) for various particles. [7]

5.2 Surface Damage

The surface region of the detector and microelectronic structures in chips contains silicon oxide, which is a product of detector passivation. Displacement damage does not lead to macroscopic changes in the surface layer. However, ionization in the oxide is not fully reversible and can cause steady deterioration of detector properties. This process is demonstrated in Figure 5.3.

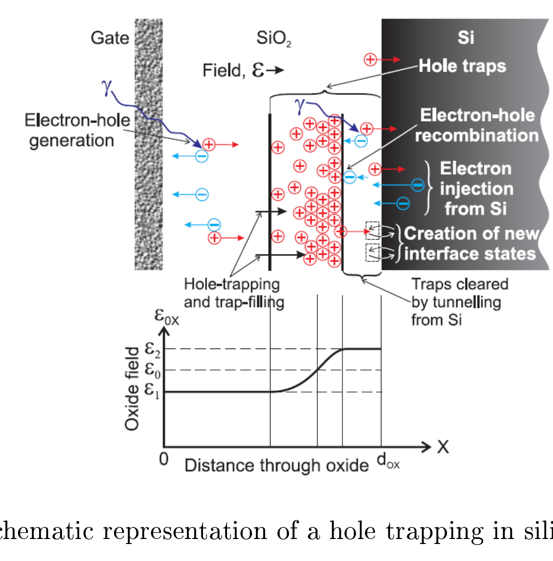

Figure 5.3: Schematic representation of a hole trapping in silicon oxide. [14]

After creating the electron-hole pairs in the oxide, most of the pairs recombine immediately. Nevertheless, electrons have high mobility in the oxide and they are collected by a positive electrode. On the other hand, holes have very low mobility and if they arrive into the region between silicon and oxide, they may be permanently trapped.

Trivalent silicon atoms with one dangling bond are also the source of positive charges in the surface layer. These positive charges lead to the flat band voltage growth, which is also dependent on the voltage applied to the surface.

Another effect is the generation of the interface states. These lead to the surface generation current, which is proportional to the surface area of the sensor. Surface damage can be annealed at a temperature above 150 °C; however, part of the oxide charge is stable. [12]

5.2.1 Surface Effects in MOSFETs

Radiation damage in MOS transistors is primarily caused by ionization damage in the oxide layer. As was mentioned above, trapping of holes in the oxide leads to the gate threshold voltage change and to the creation of a leakage path, which in the NMOS case results in parasitic transistors as illustrated in Figure 5.4. This effect can be reduced by using a different layout of transistors ("enclosed layout transistors"), which are for example mentioned in [1].

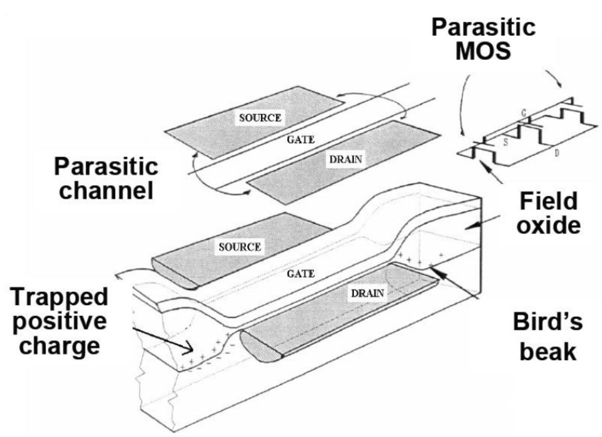

Figure 5.4: Schematic view of a NMOS transistor and building up of a leakage path. [16]

5.3 Radiation Damage in Sensor

Radiation damage in sensor is dominated by the bulk damage and results in deterioration of detector properties.

5.3.1 Increase in Leakage Current

The reverse bias current I is a linear function of the fluence Φ. For fully depleted detector it can be written as:

$$\frac{\Delta I}{V} = \alpha\Phi, \tag{5.1}$$

where α is the current-related damage rate constant and V is the depleted volume of the detector. The damage constant α is independent of the initial resistivity of silicon, the concentration of other dopants like oxygen or carbon, the production process of the sensor and the particles used for irradiation. This fact is demonstrated in Figure 5.5.

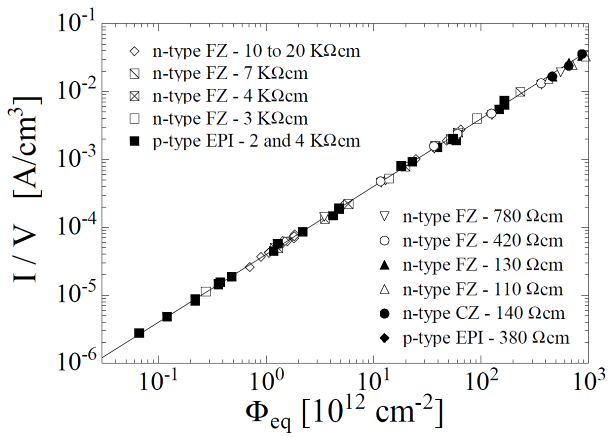

Figure 5.5: Dependence of the leakage current on fluence for various materials (FZ = float-zone, EPI = epitaxial). [7]

After irradiation, the leakage current anneals with time, with higher temperature faster as shown in Figure 5.6.

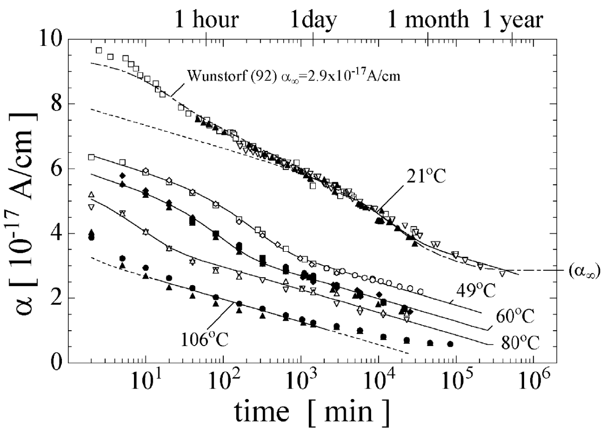

Figure 5.6: Current related damage rate α as a function of the cumulated annealing time at different temperatures. [9]

This strongly temperature-dependent behavior of the current-related damage rate can be described by

$$\alpha(t) = \alpha_i \exp(-\frac{t}{\tau_i}) + \alpha_0 - \beta \ln(\frac{t}{t_0}), \tag{5.2}$$

where

$$\frac{1}{\tau_i} = k_{i,0} e^{-E_i/kT_a}, \tag{5.3}$$

where T_a is annealing temperature and α_i, α_0, $k_{i,0}$, β, E_i are parameters, which were fitted and can be found in [12].

5.3.2 Changes in the Depleted Region

The net doping or effective doping is the difference between the donor-like states and the acceptor-like states and it can be determined from the full depletion voltage V_{depl}:

$$|N_{eff}| = \frac{2\varepsilon_0 \varepsilon_{si} V_{depl}}{ed^2}, \tag{5.4}$$

where d is the thickness of detector.

There are two contributions, which have an effect on doping characteristic of the irradiated detector. Displacement damage produces acceptor-like defects, which are occupied by electrons created by thermal excitation, and removes donor type defects. In Figure 5.7, the fluence dependence of the effective doping and of the depletion voltage are plotted. As can be seen for the n-doped material, it decreases exponentially. At a fluence of $\Phi = (2-5) \times 10^{12}\text{cm}^{-2}$

[12], the two contributions are balanced and the effective doping concentration has almost vanished ("type inversion"). With further irradiation, the absolute effective doping concentration increases again, but now like in a p-doped material.

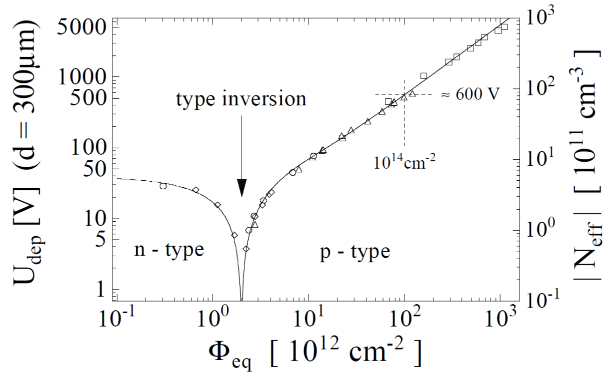

Figure 5.7: Change of the full depletion voltage and of the effective doping measured immediately after irradiation. [7]

The behavior of the irradiated detector is best described by the so-called Hamburg model [12]:

$$N_{eff} = N_{eff,0} - [N_C(\Phi) + N_a(\Phi, T_a, t) + N_Y(\Phi, T_a, t)] , \tag{5.5}$$

where $N_{eff,0}$ is the effective doping at a zero fluence and N_C, N_a, N_Y are variables discussed below.

Stable damage

N_C is not dependent on annealing time and temperature, and therefore is called the stable damage. According to the Hamburg model, it can be expressed as:

$$N_C(\Phi) = N_{C,0}(1 - e^{-c\Phi}) + g_c\Phi. \tag{5.6}$$

The first term describes the donor removal. $N_{C,0}$ is the initial concentration of removable donors. The removal constant c fluctuates for different materials and its values are in the range of $c = (1-3) \times 10^{-13}\text{cm}^2$ [12]. However, the product of both values (called the initial donor removal rate) is constant and has a value of $N_{c,0} \times c = (7.5 \pm 0.6) \times 10^{-2}\text{cm}^{-1}$. The second term describes the acceptor formation. The typical value for the acceptor introduction rate g_c is $g_c = 1.5 \times 10^{-2}\text{cm}^{-1}$ [13].

Beneficial annealing

The variable N_a in Equation 5.5 specifies the beneficial or short-term annealing. It is represented by a sum of several exponentials, but it can be approximately expressed as:

$$N_a \approx g_a \Phi e^{-t/\tau_a}, \tag{5.7}$$

where the prefactor g_a was experimentally determined as $g_a = (1.81 \pm 0.14) \times 10^{-2}\text{cm}^{-1}$[12]. The temperature-dependent decay time is expressed by the Arrhenius relation:

$$\frac{1}{\tau_a} = k_{a,0} e^{-E_a/kT_a}, \tag{5.8}$$

where E_a means the activation energy and $k_{a,0}$ is a constant dependent on the type of silicon. This part is not significant for the long-time experiments.

Reverse annealing

The last term in Equation 5.5 is the reverse annealing (or anti-annealing). Its behavior is opposite to the beneficial annealing and it describes the increase of the depletion voltage after some weeks. Although the exact function has been the subject of many discussions, the commonly used parametrization is given by:

$$N_Y = g_Y \Phi (1 - \frac{1}{1 + t/\tau_Y}), \tag{5.9}$$

with $g_Y = (5.16 \pm 0.09) \times 10^{-2}\text{cm}^{-1}$[12] and a temperature-dependent time constant:

$$\frac{1}{\tau_Y} = k_{Y,0} e^{-E_Y/kT_a}, \tag{5.10}$$

where the activation energy E_Y and $k_{Y,0}$ is a constant dependent on the type of silicon.

The whole annealing process is nicely demonstrated in Figure 5.8.

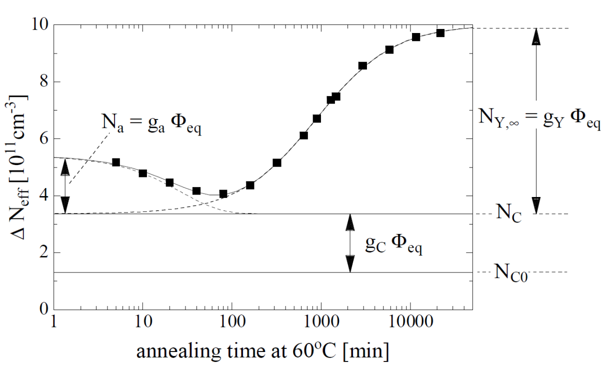

Figure 5.8: Typical annealing behavior at the temperature of 60°C. [7]

5.3.3 Charge Trapping

Radiation-induced defects are responsible for the so-called trapping centers, which trap the signal for a time longer than the charge collection time and reduce the collection efficiency. A parameter describing this effect is the trapping time τ_t and it is inversely proportional to the fluence:

$$\frac{1}{\tau_t} = \frac{1}{\tau_{t,\Phi=0}} + \gamma\Phi. \tag{5.11}$$

The coefficient γ is dependent on the particles used for irradiation.

Since it was shown that after a fluence of $10^{14}\mathrm{cm}^{-2}$ about 90% of signal can be collected, the charge trapping is less problematic than the other effects mentioned before. On the other hand, it must be taken into consideration in the spectroscopic applications and detectors must be frequently recalibrated.

5.4 Improvement

5.4.1 Process Technology

As was shown in Chapter 5.3.2, if the sensor is irradiated above the type inversion, the full depletion voltage is proportional to the fluence. Therefore, the detector should be operable at high voltages up to several hundred volts. It was shown that the use of a proper geometry of a guard ring results in a considerable improvement and the detector can be operational up to 500 volts [7].

5.4.2 Operational Conditions

In some applications (for example LHC), the full depletion voltage can exceed thousand volts after some years. However, it is impractical to increase the operational voltage into this range. It is possible to use partially depleted sensor; nevertheless, this leads to decrease of the electrical signal.

If the sensor is going to be used for several years, the cooling is also critical to keep the reverse current at a tolerable level. However, a few days or weeks without cooling are desirable, but this time period must be short enough to keep the detector in the phase of beneficial annealing.

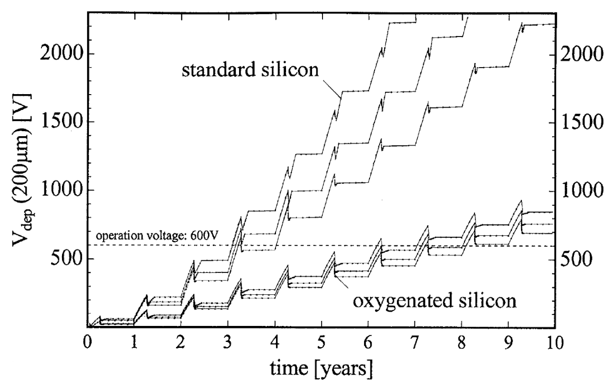

Figure 5.9: Damage projection of the full depletion voltage of the ATLAS pixel detector. [17]

An example of damage projection of the full depletion voltage of the ATLAS pixel detector can be seen in Figure 5.9. Each year is divided into three periods. The first 100 days of the year is the data-taking period. The LHC is running and the full depletion voltage of the detectors is increasing. The next period is the maintenance period. During this time the LHC and its cooling system are shut down. During these two weeks the beneficial annealing takes place. In the later years, the reverse annealing is also visible. During the rest of the year the LHC is not running, but the cooling system is switched on and there is no change in the full depletion voltage. [12]

5.4.3 Choice of Starting Material

It was shown [9], that the oxygen-enriching can be one of the possible means how to increase radiation hardness of the sensor. The main reason is the reduction of the introduction rate of the stable damage g_c. The constant g_c is reduced by a factor of 4 with respect to the standard FZ silicon [12], as indicated in Figure 5.10.

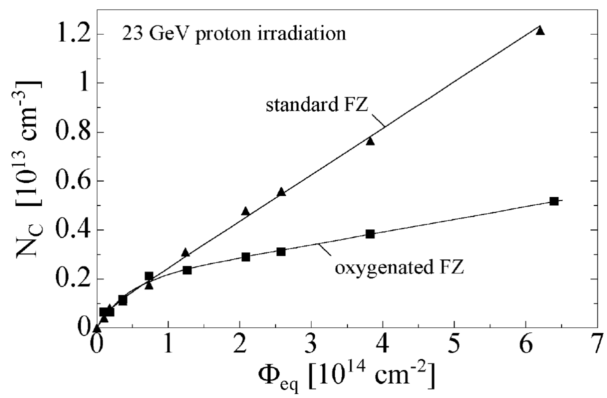

Figure 5.10: Stable damage for standard and oxygenated FZ silicon after 23 GeV proton irradiation. [9]

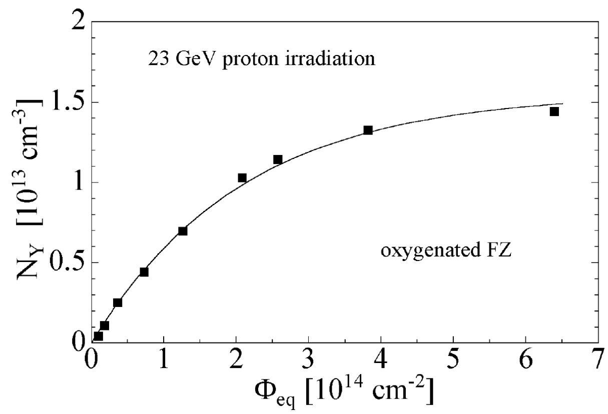

Figure 5.11: Reverse annealing of the oxygen enriched FZ silicon after 23 GeV proton irradiation. [9]

The reverse annealing is also changed after oxygenation, which is demonstrated in Figure 5.11. The constant describing the reverse annealing g_Y is reduced by a factor of 2 and the time constant is doubled [12].

These effects are related to the point defects, because there is no change of the damage parameters after neutron irradiation. However, the mechanism is not yet fully understood.

Chapter 6

Measurement of Radiation Damage in CMOS structures

The CMOS transistors are widely used in detector electronics. The purpose of this chapter is to present results of the CMOS transistors properties measurement and to study the changes of these properties after irradiation. The behaviour of the complex electronic circuit on a readout chip can be extrapoled from the behaviour of its building blocks - transistors.

6.1 Measurement Setup

For the measurement, eight test structures (TS0 - TS7) were manufactured. Each test structure differs in a type of transistor and insulation from the bulk material. A detailed view of the test structures can be seen in Figure 6.1.

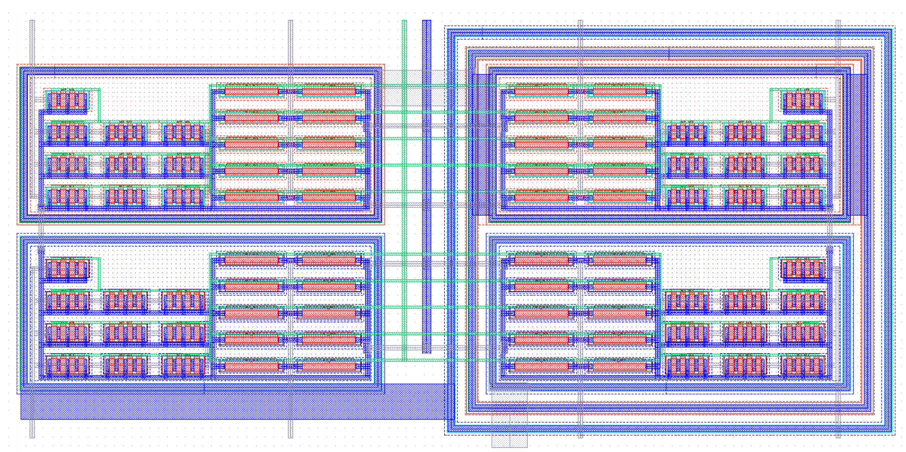

Figure 6.1: A detailed view of the test structures.

The test structures were manufactured using the commercial 150 nm CMOS technology on p-type substrate. Every structure includes ten identical MOS transistors connected in parallel to increase the effects of radiation. Half of the test structures were placed in deep n-wells (DNW) for better insulation. The parameters of the test structures are summarized in Table 6.1.

Test structure	Transistor	Width	Length
TS0	NMOS	6 μm	600 nm
TS1	NMOS	600 nm	6 μm
TS2	NMOS-DNW	6 μm	600 nm
TS3	NMOS-DNW	600 nm	6 μm
TS4	PMOS	6μm	600 nm
TS5	PMOS	600 nm	6 μm
TS6	PMOS-DNW	6 μm	600 nm
TS7	PMOS-DNW	600 nm	6 μm

Table 6.1: Types and dimensions of the test structures.

The thickness of the gate oxide was 3 nm. Test structures were irradiated for 72 hours from the ^{60}Co source, which provides 1.17 and 1.33 MeV γ-rays. The total received dose was 1.5 Mrad. After irradiation, the testing structures were left to anneal at the room temperature of $21.4 \pm 0.2\,^{\circ}$C.

The measurement of Voltage-Ampere (VA) characteristics and current consumption was repeated every 13 minutes during both irradiation and annealing. As the source of the gate voltage V_{GS} and the drain-source voltage V_{DS} Keithley 237 SMUs devices were used. The Keithley 2614B SMU was used as a source for bias ring.

6.2 Measurement Results

Measured data were analyzed in the ROOT visualization package.

6.2.1 VA characteristics

The measured VA characteristics for NMOS test structures (TS0-TS3) can be seen in Figure 6.2 and Figure 6.3. Each curve represents the VA characteristic for a given gate voltage V_{GS}, which varied from 0 V to 1.8 V in 0.05 V steps.

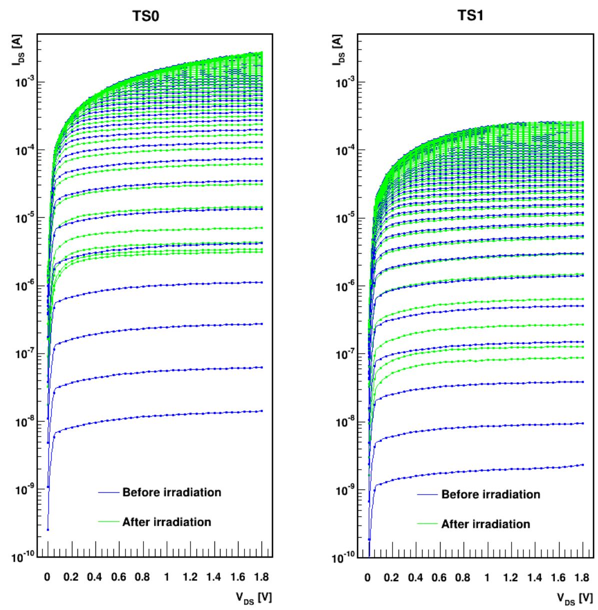

Figure 6.2: VA characteristics for TS0 and TS1.

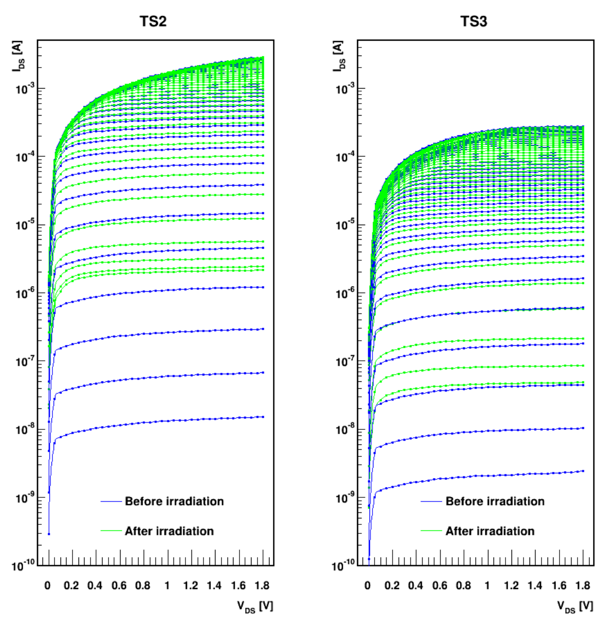

Figure 6.3: VA characteristics for TS2 and TS3.

As can be seen, the VA characteristics after irradiation are shifted as expected. A difference in VA characteristics between TS0,2 and TS1,3 is evident from the figures. It is caused by different type of transistors (combination of different lengths/widths) in test structures. Transistors that form TS0 and TS2 are multi-finger and show higher threshold voltage shift after irradiation. Also the VA characteristics shift of those test structures that were placed in deep n-wells is smaller than of those that were not. It is due to the better insulation from the surrounding bulk material.

The VA characteristics for PMOS test structures (TS4-TS7) can be seen in Figure 6.4 and Figure 6.5. The gate voltage V_{GS} varied from 1.8 V to 0 V in 0.05 V steps.

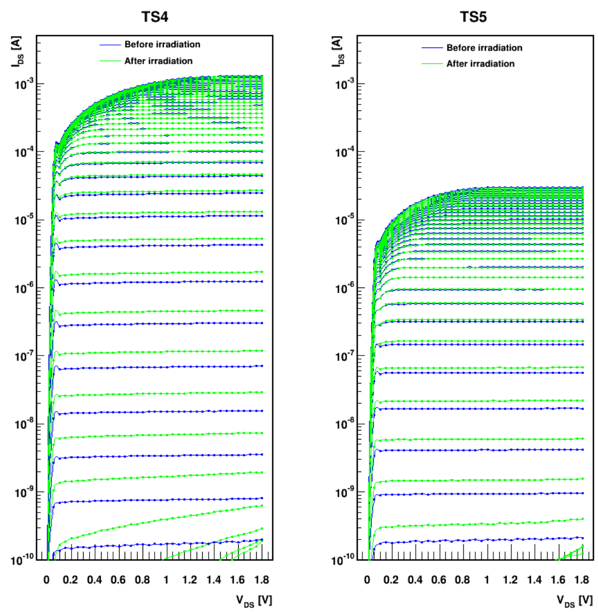

Figure 6.4: VA characteristics for TS4 and TS5.

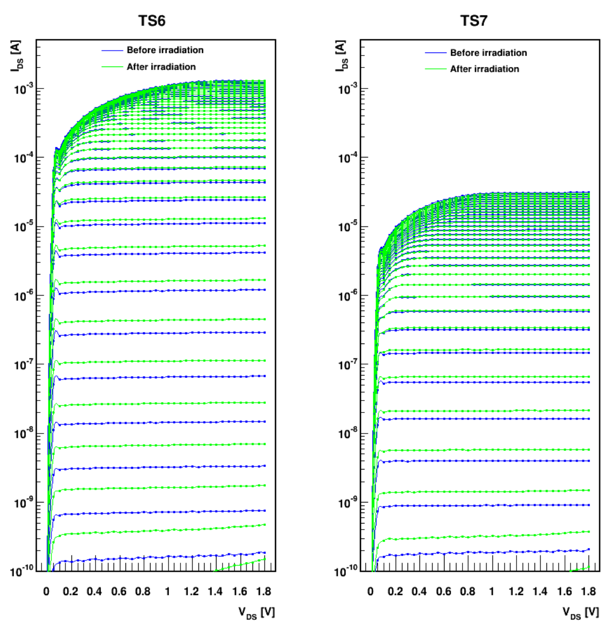

Figure 6.5: VA characteristics for TS6 and TS7.

As can be seen, the VA characteristics for PMOS transistors after irradiation are shifted. However, the shift is much smaller than that for NMOS transistors. It is because in PMOS, electrons should be trapped in the oxide (which does not happen) in order to produce a conductive channel, while in NMOS holes are trapped as was discussed in Chapter 5.2. One more effect is observable - at low gate voltage (when the channel is open) the current dropped after irradiation. It is probably due to the degradation of the majority charge carrier mobility; however, it may be a subject of further research.

6.2.2 Threshold Voltage

In a simple model a threshold voltage V_{TH} can be obtained by fitting the data using the equation [8]:

$$I_{DS} = \frac{K_P}{2}\frac{W}{L}(V_{GS} - V_{TH})^2, \tag{6.1}$$

where W is the width of the transistor, L is its length, K_P is the transconductance parameter and $V_{GS} = V_{DS}$. Figure 6.6 shows the measured data for the NMOS transistors and Figure 6.7 show the data for the PMOS transistors.

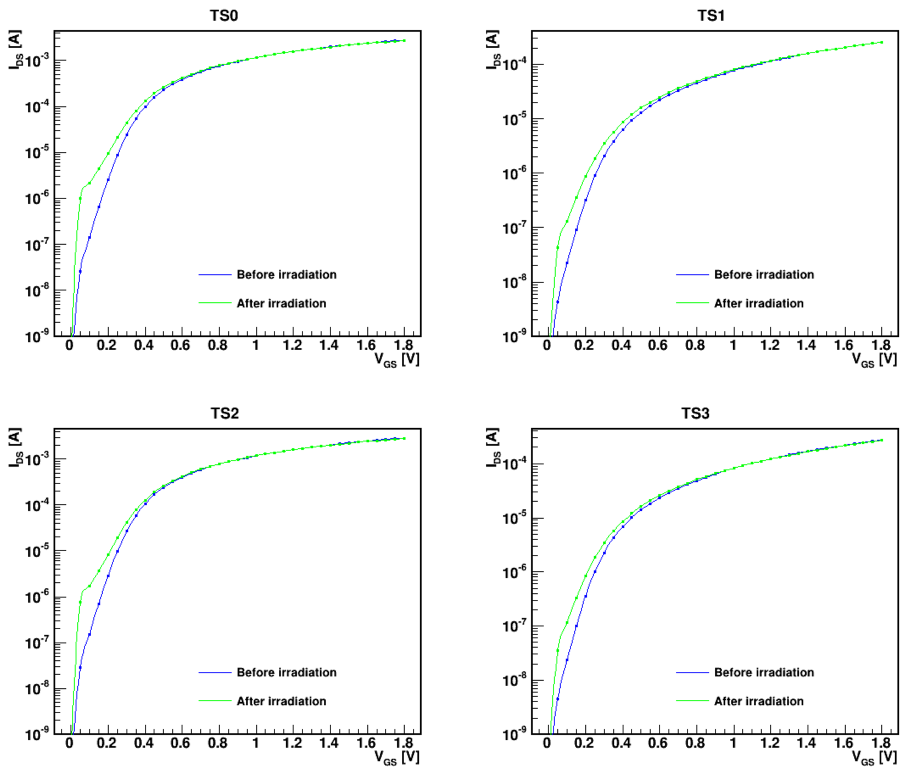

Figure 6.6: Dependence of current on the gate voltage for $V_{GS} = V_{DS}$, NMOS type.

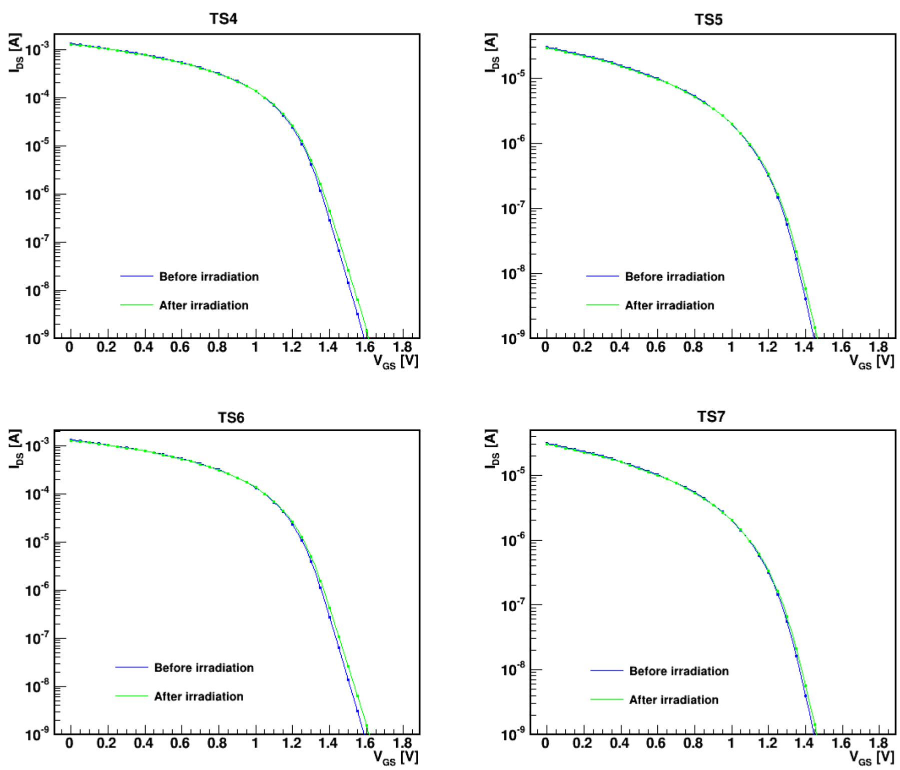

Figure 6.7: Dependence of current on the gate voltage for $V_{GS} = V_{DS}$, PMOS type.

Measured data do not show a clear parabolic dependence and the threshold voltage can not be sufficiently obtained, and therefore, a further study of the deep-submicron transistor behaviour is required. The presented simple parabolic dependence does not work very well with small transistors.

6.2.3 Current Consumption

The current consumption of an analog and digital part of the chip is shown in Figure 6.8. As can be seen, the current consumption of the digital part of the chip increased significantly after irradiation, then saturated and it gradually decreased after the interruption of the irradiation, which is a proof of annealing.

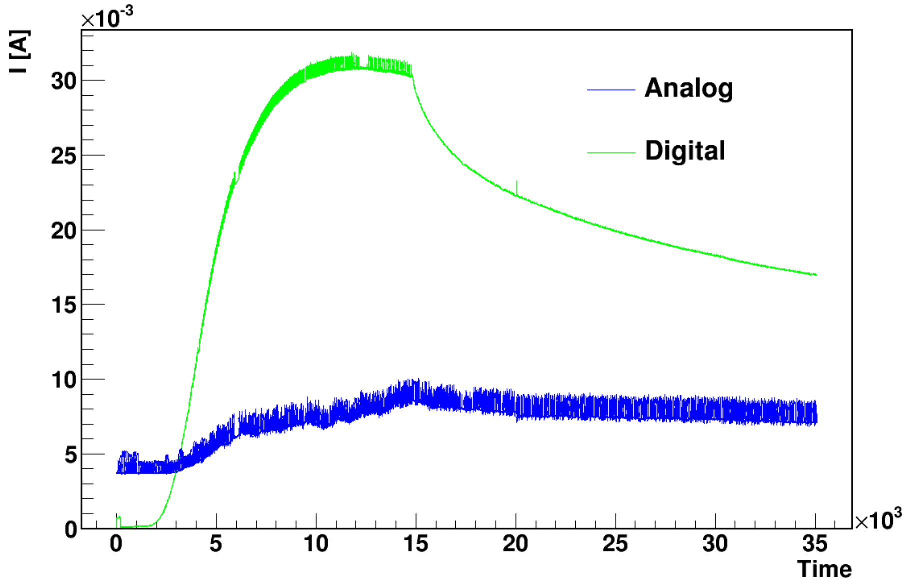

Figure 6.8: Current consumption during the measurement.

Chapter 7

Summary

The main observations obtained in the present thesis are following:

- The source-drain current measured in VA characteristics is growing with the irradiation dose, as expected.
- Various test structures have been evaluated. The attention have been focused namely on different types (NMOS, PMOS), performance and topology of transistors.

The transistor threshold voltage can not be exactly established, because the simple parabolic dependence does not fit well obtained data. Further study of the deep-submicron transistor behaviour is necessary.

The obtained original results have been presented on conferences VCI 2013 (http://vci.hephy.at/) and IWORID 2013 (http://www.synchrotron-soleil.fr/Workshops/2013/IWORID2013). These results attract interest of professional audience namely because commercial deep-submicron technology with 150 nm is today in the focus of ASIC developers and has a wide spectrum of applications. The study also provides insight into the dynamics of ionization damage of field oxides. The measured VA characteristics of test structure transistors and the total current consumption of the sample under study indicate that ionization damage at certain gamma-radiation dose saturates.

This work is a preparation for the further research of the radiation hardness of semiconductor detectors. During this work I have expanded my knowledge also in the use of ROOT visualization package and I learned many practical skills in semiconductor circuits evaluation.

In the future, I would like to work on the development of the radiation hardened detectors, because the improvement of detectors will be crucial for future experiments in particle physics and for practical applications.

Bibliography

[1] BARBERO, M. Advanced electronics and signal processing lectures - radiation damage effect. PDF presentation. http://hep1.physik.uni-bonn.de/fileadmin/Teaching/Advanced_Electronics___Signal_Processing/MB_Chapter7_Radiation_Damage_Effect.pdf, [online 5.7.2013].

[2] CERN. High school teachers at cern. http://teachers.web.cern.ch/teachers/archiv/hst2000/teaching/expt/muons/cascades.htm, [online 24.6.2013].

[3] HÖNNIGER, F. *Radiation Damage in Silicon - Defect Analysis and Detector Properties*. PhD thesis, Universität Hamburg, 2007.

[4] INSPIRE. the high energy physics information system. https://inspirehep.net/record/1236817/plots, [online 8.6.2013].

[5] KNOLL, G. F. *Radiation Detection and Measurement*, 3rd ed. John Wiley and Sons, 2000.

[6] LEROY, C., AND RANCOITA, P.-G. *Principles of Radiation Interaction in Matter and Detection*, 2nd ed. World Scientific, 2009.

[7] LINDSTRÖM, G., MOLL, M., AND FRETWURST, E. Radiation hardness of silicon detector - a challenge from high energy physics. *NIM-A 1* (1998), 18.

[8] MENOUNI, M., ET AL. 65 nm process irradiation tests. PDF presentation, 7.5.2013.

[9] MOLL, M. *Radiation Damage on Silicon Particle Detector - microscopic defects and macroscopic properties*. PhD thesis, Universität Hamburg, 1999.

[10] OKTYABRSKY, S., AND YE, P. D. *Fundamentals of III-V Semiconductor MOSFETs*. Springer, 2010.

[11] PRŮŠA, P., AND GERNDT, J. *Detektory ionizujícího záření*. Česká technika, 1995.

[12] Rossi, L., et al. *Pixel Detector: From Fundamentals to Applications.* Springer, 2006.

[13] Spieler, H. *Semiconductor Detector Systems.* Oxford University Press, 2005.

[14] Čarná, M., et al. Radiation hardness evaluation of the commercial 150 nm cmos process using 60co source. *15th IWORID 2013 Workshop, Paris* (2013).

[15] Wikipedia. The free encyclopedia. https://en.wikipedia.org/wiki/Main_Page, [online 20.7.2013].

[16] Wirth, G. Tid effects and modeling in integrated circuits. PDF presentation. http://werice2012.ieav.cta.br/Apresenta%E7%F5es/31/31Out2012%20-%20Gilson%20Wirth.pdf, October [online 30.6.2013].

[17] Wundstorf, R. Radiation tolerant sensors for the atlas pixel detector. *Nuclear Instruments and Methods in Physics Research A 466* (2001), 327–334.